Phase transitions in thin films with competing surface fields and gradients

Lijun Pang,[1] D. P. Landau,[1] and K. Binder[2]
[1]*Center for Simulational Physics, Department of Physics and Astronomy, The University of Georgia, Athens, Georgia 30602-2451, USA*
[2]*Institut für Physik, Johannes Gutenberg Universität, Staudinger Weg 7, D-55099 Mainz, Germany*
(Received 26 July 2011; published 20 October 2011)

As a generic model for phase equilibria under confinement in a thin-film geometry in the presence of a gradient in the field conjugate to the order parameter, an Ising-lattice gas system is studied by both Monte Carlo simulations and a phenomenological theory. Choosing an $L \times L \times D$ geometry with $L \gg D$ and periodic boundary conditions in the x,y directions, we place competing surface fields on the two $L \times L$ surfaces. In addition, a field gradient g is present in the z direction across the film, in competition with the surface fields. At temperatures T exceeding the critical temperature of the interface localization-delocalization transition, one finds a phase coexistence between oppositely oriented domains, aligned parallel to the surface fields and separated by an interface in the center of the film, for small enough g. For a weak gradient, a second-order transition to a monodomain state occurs, but it becomes first order if g exceeds a tricritical threshold. For sufficiently large gradients, another domain state becomes stabilized with domains oriented antiparallel to the surface fields.

DOI: 10.1103/PhysRevE.84.041603 PACS number(s): 68.08.Bc, 05.70.Np, 05.10.Ln

I. INTRODUCTION

The phase behavior of systems confined in a thin-film geometry is of interest for various applications in materials science and nanotechnology (e.g., [1,2]) and simultaneously represents a challenging problem of statistical thermodynamics. Thin films can provide protective coatings of surfaces, and can also be technologically important due to their functional properties (including optical, electronic, and mechanical properties) [3,4]. However, we shall not dwell further on such applications of thin films here but rather consider them only as a generic problem of the statistical mechanics of heterogeneous condensed matter systems. Because of the reduced dimensionality of such quasi-two-dimensional systems, effects due to statistical fluctuations are very important, and the interplay between finite-size and surface effects is responsible for phenomena distinct from what is found in the bulk (capillary condensation or evaporation of fluids in slit capillaries, wetting, and interface localization-delocalization transitions, etc.; see, e.g., [5–10] for reviews).

An additional complication arises when a gradient in some variable is maintained in the direction across the film. For instance, by coupling the lower and upper boundaries of a thin film to thermal reservoirs at different temperatures, a temperature gradient (and heat flux across the system) can be maintained. However, here we shall consider only the simpler case of a fluid film in a gravitational field (or the related cases of a ferromagnetic thin film in a magnetic-field gradient or a binary mixture in a gradient of the chemical potential difference between the species). Unlike the case of temperature gradients, no transport of heat or matter is implied by such gradients, and instead of steady states (far from thermal equilibrium), one still has full thermal equilibrium, although the state of the system clearly is not homogeneous in the direction in which the field gradient acts. We note that in binary liquid mixtures, the concentration gradients caused by gravity are indeed enough to cause unconventional patterns during phase separation processes [11], and the creation of anisotropic microporous membranes produced via diluent evaporation from the top surface of a polymer blend film [12] is another instance when composition gradients of a species in a multicomponent system are of interest. Of course, theoretical modeling of such systems will require somewhat more complexity than the simple Ising model that will be studied here as a first step. But these examples serve to illustrate the point that systems exposed to various gradients are already studied in various contexts.

So far, this problem has only been briefly discussed within the framework of Landau theory [13] and by density matrix renormalization calculations for an Ising strip (i.e., a $D \times L$ geometry with $L \to \infty$) [14]. In contrast, thin Ising films without gradients have been studied extensively [15–29]. Thus, to improve the understanding of the phase behavior of Ising-type systems in the presence of gradients, we present the first Monte Carlo study of this problem in the present paper. In addition, we present two phenomenological theoretical approaches to the problem in order to facilitate the theoretical interpretation of the Monte Carlo results (Sec. II). We have worked out a low-temperature approximation for the transition from the monodomain states of the thin film to the gradient-dominated domain state, and we also provide a treatment in terms of the capillary wave Hamiltonian approximation [30–32] for small gradient g. In Sec. III, we present and interpret the numerical results from our simulations, while Sec. IV briefly offers some conclusions.

II. THEORETICAL BACKGROUND

A. Model and low-temperature analysis

Following Rogiers and Indekeu [13], we consider an Ising Hamiltonian in an $L \times L \times D$ geometry, applying periodic boundary conditions in the x,y directions and assuming two free surfaces at which surface fields H_1, H_D act,

$$\mathcal{H} = -J \sum_{\langle i,j \rangle} S_i S_j - H \sum_i S_i - H_1 \sum_{i \in 1} S_i - H_D \sum_{i \in D} S_i + g \sum_{n=1}^{D} (2n - 1 - D) \sum_{i \in n} S_i, \quad S_i = \pm 1. \tag{1}$$

Here, we have also included a coupling to a bulk field H and a linearly varying field with a constant gradient g. In the absence of this "gravitation-like" field, the problem is already rather intricate if $H_D \neq -H_1$, so we confine ourselves to the strictly antisymmetric case, $H_D = -H_1 > 0$. Note that the Hamiltonian is constructed such that for $H = 0$, no direction of the magnetization is singled out. Therefore, phase coexistence in our system will occur exclusively for $H = 0$, as in the bulk. Note that we did not assume any modification of the nearest-neighbor exchange constant J between pairs of spins in a surface plane, and hence the model (for $g = 0$ and in the limit $D \to \infty$) exhibits a second-order wetting transition [33,34].

In the following, we consider a simple cubic lattice and take the lattice spacing as our unit of length.

To provide a qualitative understanding of the phase behavior of this model, we start from a quasimacroscopic description of the system, which should be accurate for $D \to \infty$ and at low enough temperatures (Fig. 1). The free energies per lattice plane parallel to the walls can be estimated as follows:

$$f_1 \cong D f_b + g m_b D^2/2 + f_{\rm int} - 2|H_1| m_1, \text{ state (1)}, \quad (2)$$

where f_b is the free energy of the corresponding bulk system (which has bulk magnetization m_b). The second term on the right-hand side of Eq. (2) is an estimate of the gradient energy [which neglects any deviation of the magnetization profile $m(z)$ from $-m_b$ on the left side of the interface or of $m(z)$ from $+m_b$ on the right side, respectively]. The interface free energy is denoted as $f_{\rm int}$ (neglecting any possible "renormalization" of this term by the gradient g). The last term describes the Zeeman energy due to the surface fields, where $m_1 = -m_D$ is the magnetization in the layer where the surface fields act. Effects on the free energy due to "missing neighbors" at the walls are also neglected [these effects would have a similar magnitude in all these states (1), (2), and (3)].

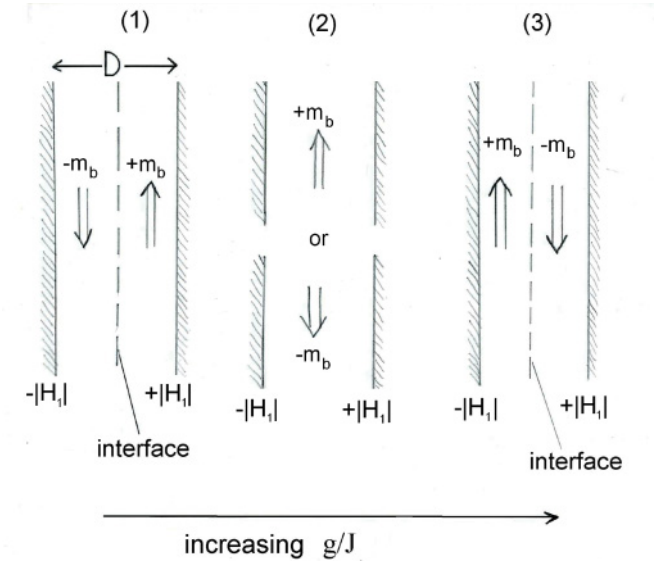

FIG. 1. Schematic description of the sequence of phases observed for $D \to \infty$ in the temperature regime $T_w < T < T_{cb}$ when the strength of the field gradient g/J increases. For small enough g/J, the surface fields dominate, and there are two domains, separated by an interface parallel to the walls [state (1)]. In this state, the sign of the magnetization and of the surface field at the adjacent wall are the same, and the magnitude of the magnetization equals the value in the bulk (m_b). In state (2), the gradient energy essentially compensates for the surface effects, yielding a degenerate state with the entire film being predominantly positively ($+m_b$) or negatively ($-m_b$) magnetized. In state (3), the gradient energy dominates: there are two domains of opposite magnetization, but the signs are opposite to that of the surface field at the adjacent wall.

In state (2), no interface is present, and both contributions due to the gradient vanish, as does the Zeeman energy due to the surface field. Hence the result is simply

$$f_2 \approx D f_b. \quad (3)$$

Note that any effects on the free energy due to a nontrivial magnetization profile $m(z)$ near the walls are ignored, but we can again argue that these effects would be similar in all three states (1), (2), and (3), and all that matters are free-energy differences between the states in question.

Similarly, for state (3) we have

$$f_3 \cong D f_b - g m_b D^2/2 + f_{\rm int} + 2|H_1| m_1. \quad (4)$$

For large enough g, it is advantageous to have domains oriented such that they overrule the free-energy cost due to the surface fields.

Since the transition between states (1) and (2) is of second order, at least for small g (see the following section based on the interface Hamiltonian treatment), one cannot simply locate the transition between states (1) and (2) by equating their free energies: in fact, the transition occurs because the interface in state (1) for $T < T_w(H_1)$ moves gradually to one of the walls. Recall that the wetting transition temperature is the limit of the interface localization or delocalization transition $T_c(H_1, D, g = 0)$ for $D \to \infty$ [7,18,20,21],

$$\lim_{D\to\infty} T_c(H_1, D, g = 0) = T_w(H_1). \quad (5)$$

Thus, the quantitative details of the transition between states (1) and (2) require a more careful and detailed treatment. However, the transition between states (2) and (3) is discontinuous, and the corresponding transition line extends even down to $T = 0$, where the approximations involved in Eqs. (2) and (3) become legitimate. Thus we estimate this transition line $g_t(D, H_1, T)$ as follows:

$$f_2 = f_3 \Rightarrow$$
$$g_t(D, H_1, T) m_b(T) D^2/2 = f_{\rm int}(T) + 2|H_1| m_1(T). \quad (6)$$

In the ground state ($T = 0$), we simply have $m_b(0) = 1$, $f_{\rm int}(0) = 2J$, $m_1(0) = 1$, and hence

$$g_t(D, H_1, 0)/J = 4(1 + |H_1|/J)/D^2. \quad (7)$$

Monte Carlo data have been generated for the special case $D = 12$, $|H_1|/J = 0.55$, implying $g_t \approx 0.043$ in this case. At finite but low T, accurate estimates for $f_{\rm int}$ can be found from Hasenbusch and Pinn [35]. For example, for $J/k_B T = 0.46 (T/T_{cb} \approx 0.48)$, one finds $f_{\rm int}/J \approx 1.851$, and using from the actual observation of the profiles (see Sec. III) that $m_1 \approx 0.98$ and hence $g_t \approx 0.0407$. As should be clear from Eq. (6), $g_t(D, H_1, T)$ gets smaller with increasing temperature, since both $f_{\rm int}(T)/m_b(T)$ and $m_1(T)/m_b(T)$ are

decreasing functions of T. While it is possible to evaluate Eq. (6) at all $T \leqslant T_{cb}$, it is clear that the approximations made in writing down f_2, f_3 break down at temperatures at which the magnetization profile $m(z)$ develops a nontrivial structure, and the failure of Eq. (6) at $T/T_{cb} \geqslant 0.6$ is also evident from a comparison of Eq. (6) with the Monte Carlo data (see Sec. III).

B. Interface Hamiltonian treatment

In the absence of the gradient term in Eq. (1), the interface localization or delocalization transition of the Ising model on a mean-field level can be described by the following interface Hamiltonian [7,18,21]:

$$\mathcal{H}_{\rm eff}(\ell) = \int d\vec{\rho}\left[\frac{f_{\rm int}}{2}(\nabla\ell)^2 + V(\ell)\right]; \tag{8}$$

here, $\vec{\rho} = (x,y)$ denotes the coordinates in the plane of the left wall in Fig. 1 and $\ell(\vec{\rho})$ is the local distance of the (fluctuating) interface from the wall. For the case of a second-order wetting transition in the limit $D \to \infty$, the interface potential $V_0(\ell)$ is

$$\begin{aligned} V_0(\ell) = &-2a_0\delta\varepsilon\exp(-\kappa D/2)\{\cosh[\kappa(\ell - D/2)] - 1\} \\ &+ 2b\exp(-\kappa D)\{\cosh[\kappa(2\ell - D)] - 1\} \\ &+ h(\ell - D/2). \end{aligned} \tag{9}$$

Here a_0, b are phenomenological, positive constants, $\delta\varepsilon = (T_w - T)/T_w$, and κ^{-1} is a length that is of the same order as the correlation length of the order parameter in the bulk. Note that Eq. (8) implies that all bulk fluctuations in the system have been already eliminated by some coarse-graining procedures, so the only degrees of freedom left are the positions $\ell(\vec{\rho})$ of the interface separating a domain of magnetization $-m_b(T)$ on the left side of the interface from a domain with magnetization $+m_b(T)$ on the right side. Thus, the last term on the right-hand side of Eq. (9) simply represents the Zeeman energy in Eq. (1), and therefore $h = 2Hm_b(T)$. We disregard here the explicit relation of the parameters a_0, b, T_w to the parameters k_BT/J and H_1/J of Eq. (1). We also note that for the present somewhat qualitative treatment, the "local" interface Hamiltonian, Eq. (8), suffices, thus there is no need for the nonlocal theory [36].

Now we also need to translate the gradient energy in Eq. (1) to the description in terms of the interface Hamiltonian. Noting that the continuum analog of the gradient energy in Eq. (1) is

$$\text{gradient energy} = g\int_0^D dz(2z - D)m(z) \tag{10}$$

and that $m(z) = -m_b$ for $0 \leqslant z \leqslant \ell$ while $m(z) = +m_b$ for $z > \ell$, we readily obtain from Eq. (10)

$$\text{gradient energy} = -2gm_b(\ell^2 - D\ell). \tag{11}$$

Note that the gradient energy is symmetric around $\ell = D/2$, where it has a maximum of height $V_{\rm max} = gm_bD^2/2$, while it vanishes for both $\ell = 0$ and $\ell = D$.

Adding Eq. (11) to the potential in Eq. (9), $V(\ell) = V_0(\ell) + \text{gradient energy}$, we then find the equilibrium position of the interface by minimizing $V(\ell)$ with respect to ℓ, i.e., $[\partial V(\ell)/\partial\ell]_T = 0$. This yields

$$\begin{aligned} &- 2a_0\delta\varepsilon\kappa\exp(-\kappa D/2)\sinh[\kappa(\ell - D/2)] \\ &+ 4b\kappa\exp(-\kappa D)\sinh[\kappa(2\ell - D)] \\ &+ h - 2gm_b(2\ell - D) = 0. \end{aligned} \tag{12}$$

For $T \geqslant T_c(H_1, D, g)$, the only solution of Eq. (12) for $h = 0$ is $\ell = D/2$, i.e., the state (1) in Fig. 1. At $T_c(H_1, D, g)$, the second derivative of the potential for $\ell = D/2$ changes its sign; thus the condition

$$\begin{aligned} \left(\frac{\partial^2 V(\ell)}{\partial\ell^2}\right)_{T,\ell=D/2} &= -2a_0\delta\varepsilon\kappa^2\exp(-\kappa D/2) \\ &\quad + 8b\kappa^2\exp(-\kappa D) - 4gm_b = 0 \end{aligned} \tag{13}$$

yields $T_c(H_1, D.g)$, i.e.,

$$\begin{aligned} &2a_0\frac{T_c(H_1, D, g) - T_w}{T_w} \\ &\quad = -8b\exp(-\kappa D/2) + \frac{4gm_b}{\kappa^2}\exp(\kappa D/2). \end{aligned} \tag{14}$$

As is well known from previous work for $g = 0$ [7,18,21], $T_c(H_1, D, g = 0)$ approaches T_w from below; but the difference between $T_c(H_1, D, g = 0)$ and T_w is exponentially small, $\propto \exp(-\kappa D/2)$. However, when $g > 0$, we see that $T_c(H_1, D, g)$ increases rapidly, and the region where $T_c(H_1, D, g)$ exceeds T_w is already reached for an exponentially small value of g, namely $g > (2b\kappa^2/m_b)\exp(-\kappa D)$.

We now characterize the critical behavior of the interface localization-delocalization transition at $T_c(H_1, D, g)$ [or the corresponding values $\delta\varepsilon_{\rm crit}$ of $\delta\varepsilon$ in Eqs. (9), (12), and (13)]. We first recall that the inverse susceptibility χ^{-1} of the system is $[M = (L^2D)^{-1}\sum_i\langle S_i\rangle_T]$ [7,18,21]

$$\begin{aligned} \chi^{-1} &= (\partial M/\partial H)_T^{-1}, \\ &\propto [\partial^2 V(\ell)/\partial\ell^2]_T^{-1}\,|_{\ell=D/2}, \end{aligned} \tag{15}$$

and we readily conclude from Eqs. (12) and (13) that

$$\begin{aligned} &\left(\frac{\partial^2 V(\ell)}{\partial\ell^2}\right)_T^{-1}\,|_{\ell=D/2} \\ &\quad = 2a_0\kappa^2\exp(-\kappa D/2)[T - T_c(H_1, D, g)]/T_w. \end{aligned} \tag{16}$$

Equation (16) shows that for nonzero g for $T > T_c(H_1, D, g)$, we also have a "soft mode" phase, with a susceptibility that diverges exponentially with D as $D \to \infty$ [due to an amplitude factor $\exp(\kappa D/2)$] at all temperatures $T < T_{cb}$. At T_c and below, the behavior is more subtle: we expand $\sinh x \approx x + x^3/3$ in Eq. (12) to find for $T = T_c(H_1, D, g)$

$$h = \left(\frac{m}{m_b}\right)^3(\kappa D)^3\kappa[b\exp(-\kappa D) + gm_b/6\kappa^2], \tag{17}$$

where we have used the fact that $x = \kappa(\ell - D/2) = -(\kappa D/2)(m/m_b)$. From Eq. (17), we see that there are two regimes: only for $g \ll g_{\rm cross} = (6\kappa^2 b/m_b)\exp(-\kappa D)$ is the effect of the gradient negligible, and we recover the anomalous amplitude factor $\exp(-\kappa D)$ characteristic for the soft-mode

phase [21]. However, for $g > g_{\rm cross}$ there is no longer any anomalous response. Similarly, for $T < T_c(H_1, D, g)$, we find

$$x^2 = \left(\frac{\kappa D}{2}\right)^2 \left(\frac{m}{m_b}\right)^2 \approx \frac{3a_0[T_c(H_1, D, g) - T]/T_w}{12b\exp(-\kappa D/2) + (2gm_b/\kappa^2)\exp(\kappa D/2)}. \quad (18)$$

As expected, for $g \to 0$, Eq. (18) reproduces the result [21] $m \propto \exp(\kappa D/4)\sqrt{T_c(H_1, D, g) - T}$, but this anomalously large order parameter amplitude [proportional to $\exp(\kappa D/4)$] is no longer seen when g exceeds the value $g_{\rm cross} \propto \exp(-\kappa D)$. As a final caveat, we note that the mean-field critical exponents $\beta = 1/2$, $\gamma = 1$, and $\delta = 3$, which can be read off from our results for the order parameter Eq. (18), susceptibility Eq. (16), and critical isotherm Eq. (17), are not expected to describe the actual critical behavior if $g > g_{\rm cross}$. We recall that for $g = 0$, mean-field theory is self-consistent for $D \to \infty$, as a Ginzburg criterion shows [21]. Of course, Eq. (14) loses its validity when g is so large that $T_c(H_1, D, g)$ moves into the critical region of the bulk. Rogiers and Indekeu [13] suggested a finite-size scaling relation for the shift of T_c in this region,

$$(T_c(D, H_1, g) - T_{cb})/T_{cb} = D^{-1/\nu} Y(D^{\Delta_1/\nu} H_1, D^{\psi/\nu} g), \quad (19)$$

where ν is the critical exponent of the correlation length, Δ_1 is an exponent describing the critical behavior of free surfaces [37], and $\psi = \Delta + \nu$ (where Δ is the "gap exponent" in the bulk [38]). The scaling function Y has not been calculated explicitly, however. Assuming (as is corroborated by the numerical data, see Sec. III) that the curve $T_c(D, H_1, g)$ exhibits a maximum in the (T, g) plane at $T_{\rm max}$, $g_{\rm max}$, we conclude from Eq. (19) that

$$T_{\rm max} - T_{cb} \propto D^{-1/\nu}, \quad g_{\rm max} \propto D^{-\psi/\nu}. \quad (20)$$

Unfortunately, an extension of the interface Hamiltonian treatment into the bulk critical region is not at all obvious, and hence it is not attempted here.

III. MONTE CARLO SIMULATION RESULTS

In this section, we present the results of Monte Carlo simulations of the Ising model, Eq. (1), assuming a simple-cubic lattice with a thin-film thickness $D = 12$. These simulations extend previous work on interface localization or delocalization transitions in Ising models done for $g = 0$ only [20,21,23,27]. As is well known, the delocalized interface (with the average location at $z = D/2$) is a very slowly relaxing object, making it very difficult to obtain meaningful accuracy. While in previous work for $g = 0$ a comparative study of film thicknesses $D = 6$, 8, and 12 was presented [20,21], we focus here on a single thickness $D = 12$, aiming at a comprehensive study of the effects of varying the strength of the gradient energy, g. Most data have been taken for a single choice of L, $L = 128$, but in a few cases L was systematically varied in order to carry out a finite-size scaling analysis. We use $|H_1|/J = 0.55$ throughout, as in previous work [20,21], where $J/k_BT_c(H_1/J = 0.55, D = 12) = 0.2497 \pm 0.0003$ was determined. Note that at this critical temperature, $\kappa/2 \approx 0.364$ was also estimated [21], implying $\exp(\kappa D/2) \approx 78.9$. Since this value is rather large, a test of Eq. (14) by our simulations turned out to be prohibitively difficult and must be left to future work. Note also that within our accuracy, we cannot distinguish the wetting transition temperature $[J/k_BT_w(H_1/J = 0.55) \approx 0.250]$ from J/k_BT_c for $D = 12$, as quoted above. For our simulations, standard single-spin-flip Monte Carlo methods (applying the heat bath algorithm [39,40]) were used. (As is well known, in the presence of strong surface fields, the application of cluster algorithms does not offer any advantage [26].)

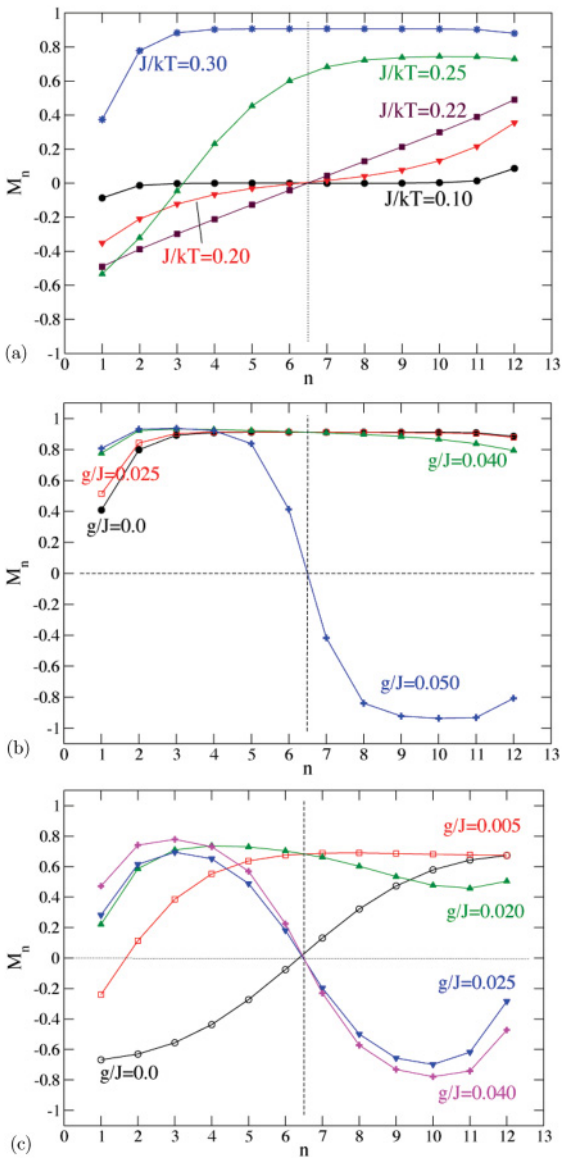

FIG. 2. (Color online) Layer magnetization m_n vs layer number n for the case $L = 128$, $D = 12$, $H_1 = -H_D = -0.55J$: (a) $g/J = 0.01$ and several choices of J/k_BT; (b) $J/k_BT = 0.303$ and several choices of (g/J); (c) $J/k_BT = 0.244$ and several choices of g/J. Note that m_n is defined only for integer values of n, and data points are connected by straight lines to guide the eye. The midplane (which, in the continuum limit where z runs from $z = 0$ to $xz = D$, has been denoted as $z = D/2$ in Sec. II) is located at $z = (1 + D)/2 = 6.5$ (vertical broken line), since for $D = 12$ there are 12 lattice planes from $n = 1$ to 12. The horizontal broken straight line highlights zero magnetization.

Figures 2(a)–2(c) show "raw Monte Carlo data" for our magnetization profiles (for technical details of these Monte Carlo simulations, the reader may also consult [20,21,39]). The case shown in Fig. 2(a) illustrates the behavior of the model as the temperature is lowered at a small but nonzero value of g. Far above T_{cb}, e.g., $J/k_BT = 0.1$, the layer magnetization m_n is zero everywhere except close to the walls, where a nonzero magnetization is induced by the surface fields. As the temperature is lowered toward T_{cb}, an interface is gradually formed in the center (but no sharp phase transition occurs). For $g/J = 0.01$ at temperatures slightly below $J/k_BT = 0.22$, the interface merely fluctuates about the center of the film. When the temperature decreases to $J/k_BT = 0.25$, however, the interface moves toward one of the surfaces until it is finally bound to the surface. For the low temperature, $J/k_BT = 0.303$, which is well below T_w, for small g/J we realize state (2) in Fig. 1. Of course, the magnetization is not strictly uniform, because it is reduced near both walls [near the wall at $z = D$, where the positive surface magnetic field acts, this reduction is less pronounced than for the opposite wall (first layer, $n = 1$), where the negative surface field and the "missing neighbor effect" act in the same direction]. These effects are neglected in the simple estimates of Sec. II1, and it is therefore clear that at the temperature of Fig. 2(a), Eq. (6) is no longer accurate. Note that the effect of g on the profiles is also very asymmetric: for increasing g, the reduction of m_n for $n = 1,2,3$ is somewhat reduced, while near the other wall g has little effect. However, when g/J becomes large (see the data for $g/J = 0.04$), the gradient starts to lead to a reduction of m_n near $n = 12$. Finally, for still larger g/J (such as $g/J = 0.05$), the transition to state (3) in Fig. 1 has occurred.

Turning now to the temperature $J/k_BT = 0.244$, a case in which $T > T_w$, we see that for $g/J = 0.0$ the interface is delocalized in the center of the film, as expected [20,21]. However, for $g/J = 0.005$, the transition from state (1) to state (2) in Fig. 1 has already occurred. For $g/J = 0.020$, we see that the gradient causes a significant reduction of m_n near $n = D$, while for $g/J = 0.025$ the transition from state (2) to state (3) in Fig. 1 has already occurred.

Since the transition from state (2) to state (3) is of first order, we encounter strong hysteresis, particularly at low temperature. The simplest recipe to deal with this problem is to apply standard thermodynamic integration methods, as described in the textbooks [39,40]. Figure 3 gives some

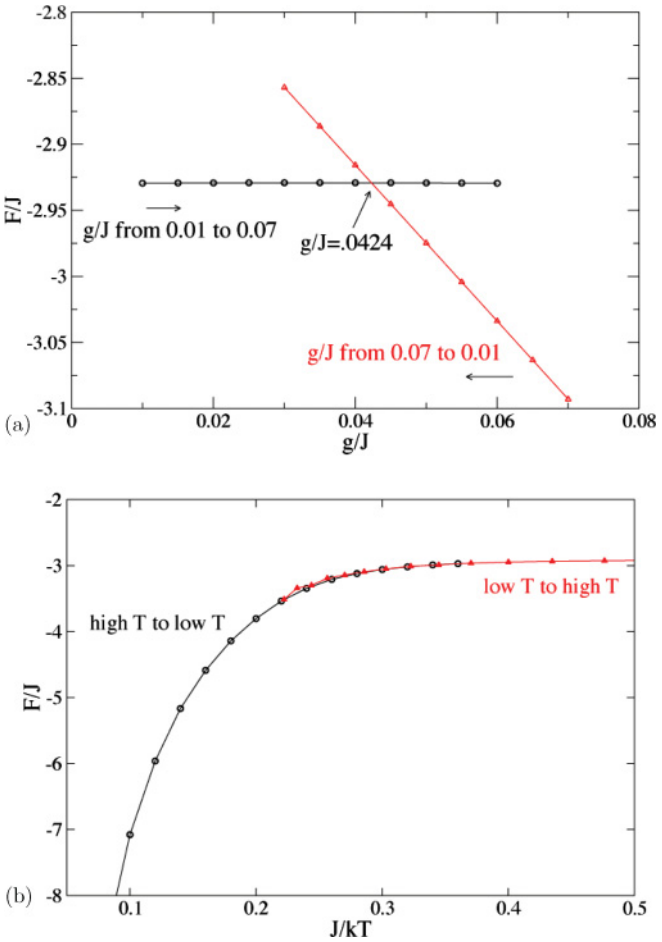

FIG. 3. (Color online) Free energy as obtained from thermodynamic integration varying g/J at constant temperature [$J/k_BT = 0.467$, $L = 256$, case (a)] and varying inverse temperature J/k_BT at constant $g/J = 0.025$ (b). In (a), the estimated transition point (at $g/J = 0.0424$) is highlighted.

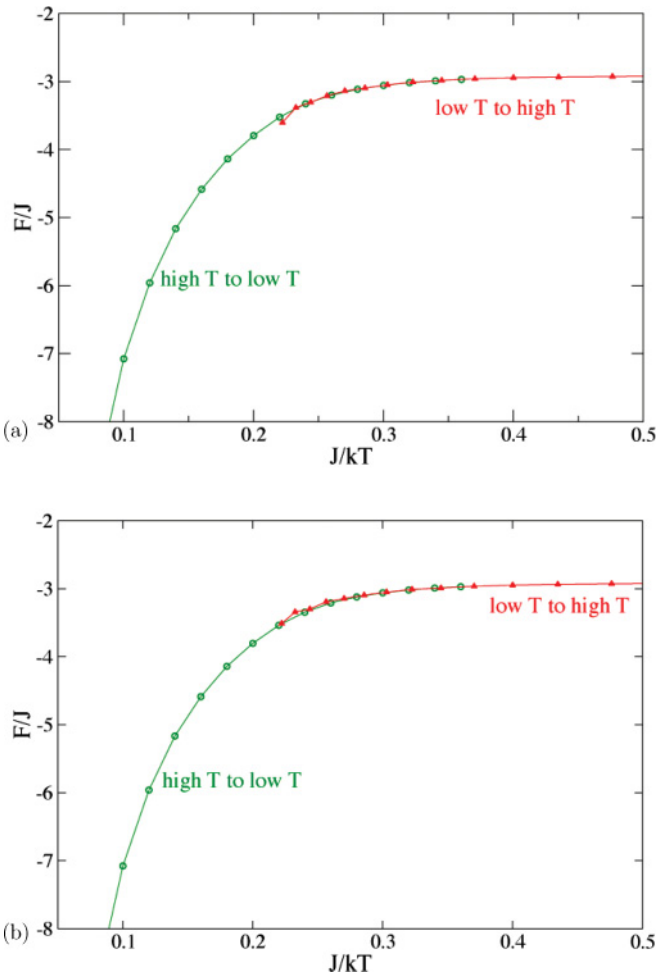

FIG. 4. (Color online) Free energy as obtained from thermodynamic integration varying J/k_BT at fixed g: (a) $g/J = 0.01$ and (b) $g/J = 0.0$.

examples: The intersection of the free-energy branches at low T when g is varied allows an accurate estimation of the transition value. However, this method breaks down near the maximum of the curve $T_c(D,H_1,g)$. Then it is necessary to carry out an integration varying J/k_BT at fixed g, rather than the other way round [Fig. 3(b)]. Unfortunately, near the tricritical point, the accuracy of this method becomes questionable since the two free-energy branches cut each other under a rather small angle. As a check of the accuracy of our procedures, we have also carried out a free-energy integration in the second-order region: there, the two curves should superimpose irrespective of in which phase [(1) or (2)] one starts, and this is indeed verified nicely (Fig. 4). While this procedure does not help to locate the transition (1)–(2) accurately, it shows that neither statistical inaccuracy of the raw data nor errors due to the numerical integration routine are a serious problem.

In the second-order regime, we expect that the phase transition should fall in the universality class of the two-dimensional Ising model. We used this hypothesis in order to locate the transition point accurately. One possibility is to attempt to locate fourth-order cumulant intersections for different values of L. As usual, the cumulant of the distribution $P_L(M)$ of the total average magnetization is defined by [41]

$$U_L = 1 - \langle M^4\rangle/3\langle M^2\rangle^2. \tag{21}$$

Figure 5 shows a resulting attempt to apply this method for $g/J = 0.015$. As was already found for the case $g/J = 0.0$ [20,21], there is considerable scatter in the intersections, and they all lie below the theoretical cumulant value [44], $U_L(T_c) = U^* = 0.610$. Thus, one can only achieve modest accuracy, $J/k_BT_c = 0.2320 \pm 0.0002$. However, while for $g = 0$ and $D = 12$ all values $U_L(T)$ were very far below this theoretical value U^* [as expected from the Ginsburg criterion [21], the asymptotic Ising critical behavior is only seen quite close to $T_c(0)$], in the present case [Fig. 5(a)] there is a much clearer trend of $U_L(T_c)$ moving toward U^* as L increases. This is in qualitative accord with the considerations of Sec. II B.

Note that despite long runs (4×10^7 Monte Carlo steps/spin), rather large statistical errors still occur. (Error bars

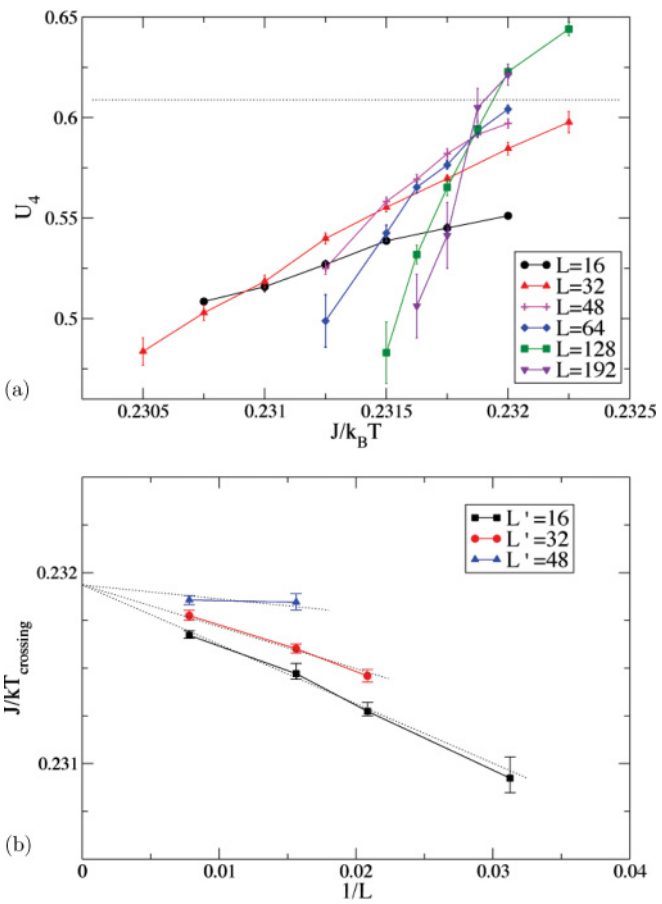

FIG. 5. (Color online) (a) Fourth-order cumulant U_L plotted vs inverse temperature for the case $D = 12$, $H_1 = -H_D = -0.55J$, $g/J = 0.015$, and several choices of L. The dotted horizontal straight line indicates the expected result [42–44] for the universality class of the $d = 2$ Ising model. (b) Extrapolation of the values of the inverse temperature J/k_BT of crossing points vs L^{-1} for different choices of the reference lattice size L'. The dashed lines are straight lines fitted to the data.

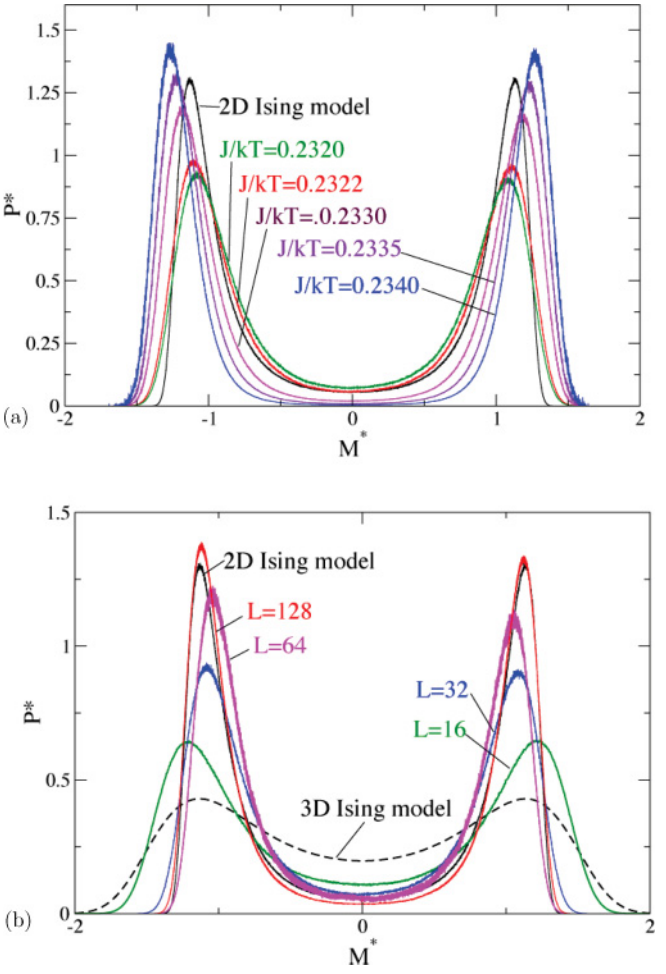

FIG. 6. (Color online) (a) Normalized probability distribution $P_L^*(M^*) = \langle M^2\rangle^{-1/2} P_L(M)$ vs $M^* = \langle M^2\rangle^{-1/2} M$ generated at $J/k_BT = 0.2322$ and reweighted to various neighboring temperatures, as indicated, compared to the planar Ising model distribution at criticality. (b) Probability distribution $P_L^*(M^*)$ vs M^* for $J/k_BT = 0.2320$ and different values of L. For comparison, $P_L^*(M^*)$ for the two- and three-dimensional Ising models are included as well.

were estimated from multiple independent runs.) Nonetheless, the convergence to the Ising value is quite clear, unlike the case of zero-field gradient, for which the convergence is quite slow (see Fig. 3 in Ref. [21]). The finite-size extrapolation of the temperatures at which the curves cross, shown in Fig. 5(b) for different size reference systems, provides a consistent estimate for the asymptotic value of the critical temperature.

As an additional approach, we followed Wilding [45] by using the full information of $P_L(M)$ and adjusting J/k_BT until a good fit of the normalized distribution $P_L^*(M^*)$ to that of the two-dimensional Ising model is obtained. However, if one does this, a good fit of the peak heights is obtained at temperatures that are clearly too low ($J/k_BT = 0.2335$), and the peak positions are clearly unreliable. We conclude that optimizing $P_L(M)$ by histogram reweighting is not an accurate method in our case [Fig. 6(a)]. However, when we study $P_L(M)$ for different L at our best estimate for J/k_BT, $J/k_BT_c = 0.2320$, we find a reasonable convergence toward the Ising distribution [Fig. 6(b)].

In view of the difficulties encountered in locating the critical points accurately (Figs. 5 and 6) and dealing with weak first-order transitions [Fig. 3(b)], only a rather rough phase diagram could be constructed in which we expected that the tricritical point occurs somewhere between $g/J = 0.020$ and 0.025.

By performing the two-dimensional histogram reweighing technique, the normalized probability distribution $P_L^*(M^*) = \langle M^2\rangle^{-1/2} P_L(M)$ vs $M^* = \langle M^2\rangle^{-1/2} M$ generated at $J/k_BT = 0.241\,67$, $g/J = 0.0204$ was reweighted to neighboring temperatures and field gradients. We find that at $J/k_BT = 0.242\,418$, $g/J = 0.020\,65$, as indicated in Fig. 7, the probability distribution is in very good agreement with the planar Ising model distribution at a tricritical point [46]. Thus, the tricritical point was roughly located in the final phase diagram shown in Fig. 8.

Note that the low-temperature approximation Eq. (6) is not quantitatively accurate for $T/T_{cb} > 0.4$, but it does reproduce the trend of the first-order transition line qualitatively. Clearly, the obtainable precision of the present work and the competing

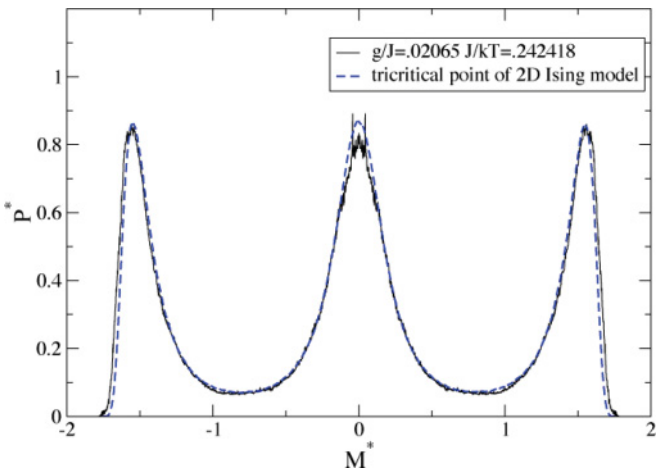

FIG. 7. (Color online) Normalized probability distribution $P_L^*(M^*) = \langle M^2\rangle^{-1/2} P_L(M)$ vs $M^* = \langle M^2\rangle^{-1/2} M$ generated at $J/k_BT = 0.241\,67$, $g/J = 0.0204$, and reweighted to $J/k_BT = 0.242\,418$, $g/J = 0.020\,65$, as indicated, compared to the planar Ising model distribution at a tricritical point [46].

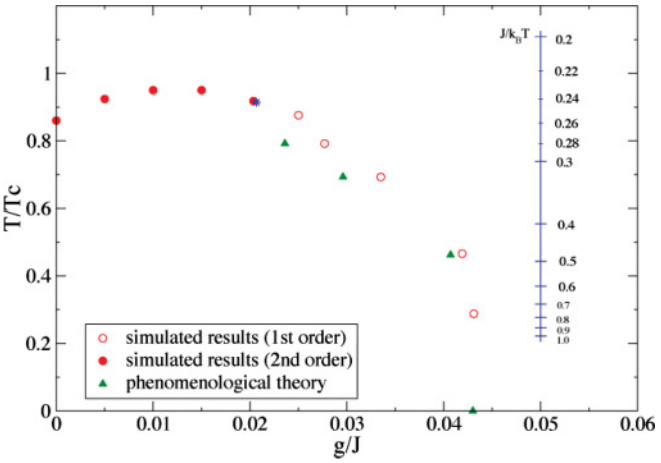

FIG. 8. (Color online) Phase diagram of the Ising thin film ($D = 12$) plotted in the plane of variables T/T_{cb} and g/J. Second-order transitions [from state (2) in Fig. 1 at low temperature to state (1) at higher temperature] are shown by full dots; first-order transitions [from state (2) to state (3)] are shown by open circles. The tricritical point is show by a star. Triangles show estimates based on Eq. (6).

finite-size crossover effects also make it impossible to attempt a meaningful test of the predictions based on the interface Hamiltonian method (which are supposed to work near $g/J = 0$).

IV. CONCLUSIONS

Monte Carlo simulations combined with finite-size studies have confirmed the qualitative features of the mean-field picture of the phase diagram of the Ising thin field with oppositely directed surface fields in the presence of a field gradient. The presence of the field gradient actually makes it easier to extract the asymptotic, i.e., infinite lattice, transition behavior even though the resolution is still somewhat limited. The phase diagram for the interface delocalization transition in a film with $D = 12$ layers is reentrant and exhibits two phase transitions for $T > T_w$. Using a phenomenological theory based on the capillary wave type interface Hamiltonian description, we argued that the anomalous features of the interface localization transition for $g = 0$ [namely that critical amplitudes depend exponentially on film thickness D, and critical behavior is mean-field-like, except for an extremely narrow region around $T_c(D)$] are removed by the presence of a very small gradient of order $g_{\rm cross} \propto \exp(-\kappa D)$. A finite-size analysis of the behavior at a moderate value of g/J provides convincing evidence that the critical behavior along the second-order portion of the phase boundary is in the universality class of the two-dimensional Ising model. We presented a low-temperature approximation that does appear to describe the actual behavior of the phase boundary at low temperatures at least semiquantitatively.

Finally, we ask the following question: Is there the possibility to study a system experimentally where a gradient competes with boundary fields such that the system undergoes an Ising-type transition in the bulk? While one might first think that a thin magnetic film in a magnetic-field gradient

would be a good candidate, we believe that it is more likely that success could be achieved in colloid-polymer mixtures, which are "Ising equivalent" systems for the study of phase transitions and interfacial phenomena [47,48]. For colloids of several μm diameter, gravity couples sensitively to the colloid density; a competing wall situation could be created if one wall is just a hard wall [10] (which exerts an entropic attraction on the colloidal particles) while the opposite wall is coated with a polymer layer (attracting the polymers in the dispersion rather than the colloids). Of course, such a system would not have the perfect Ising symmetry between the coexisting phases in the bulk, and one also cannot expect to realize "antisymmetric" walls precisely, so such a system will have more complex properties than the simple Ising system studied here.

ACKNOWLEDGMENTS

This research was supported by NSF Grant No. DMR-0810223. The simulations were performed at the Research Computer Center (RCC) at the University of Georgia. One of us (D.P.L.) is grateful to the Schwerpunkt fuer Rechnergestuetzte Forschung in den Naturwissenschaften (SRFN) of the University of Mainz for partial support of his research stays at Mainz.

[1] *Multilayer Thin Films: Sequential Assembly of Nanocomposite Materials*, edited by G. Decker and J. B. Schlenoff (Wiley-VCH, Weinheim, 2002).
[2] *Nano-Architectured and Nano-Structured Materials*, edited by Y. Champion and H. J. Fecht (Wiley-VCH, Weinheim, 2004).
[3] *Handbook of Nanostructured Thin Films and Coatings*, edited by S. Zhang, Vols. 1–3 (CRC, Boca Raton, FL, 2010).
[4] *Thin Films-Stresses and Mechanical Properties XI*, edited by T. E. Buchheit, A. M. Minor, R. Spolenak, and K. Tabashima, Materials Research Society Symposia Proceedings No. 875 (MRS, Warrendale, PA, 2005).
[5] R. Evans, J. Phys. Condens. Matter **2**, 9899 (1990).
[6] L. D. Gelb, K. E. Gubbins, R. Radhakrishnan, and M. Sliwinska-Bartkowiak, Rep. Prog. Phys. **62**, 1573 (1999).
[7] K. Binder, D. P. Landau, and M. Müller, J. Stat. Phys. **10**, 1411 (2003).
[8] M. Schön and S. Klapp, *Nanoconfined Fluids: Soft Matter Between Two and Three Dimensions* (Wiley, New York, 2006).
[9] I. Brovchenko and A. Oleinikowa, *Interfacial and Confined Water* (Elsevier, Amsterdam, 2008).
[10] K. Binder, J. Horbach, R. Vink, and A. De Virgiliis, Soft Matter **4**, 1555 (2008).
[11] Y. Jayalakshmi, B. Khalil, and D. Beysens, Phys. Rev. Lett. **69**, 3088 (1992).
[12] H. Matsuyama, M. Yuasa, Y. Kitamura, M. Teramoto, and D. R. Lloyd, J. Membr. Sci. **179**, 91 (2000).
[13] J. Rogiers and J. O. Indekeu, Europhys. Lett. **24**, 21 (1993).
[14] E. Carlon and A. Drzewinski, Phys. Rev. Lett. **79**, 1591 (1997).
[15] M. E. Fisher and H. Nakanishi, J. Chem. Phys. **75**, 5857 (1981).
[16] H. Nakanishi and M. E. Fisher, J. Chem. Phys. **78**, 3279 (1983).
[17] E. V. Albano, K. Binder, D. W. Heermann, and W. Paul, Surf. Sci. **223**, 151 (1989); J. Chem. Phys. **91**, 3700 (1989).
[18] A. O. Parry and R. Evans, Phys. Rev. Lett. **64**, 439 (1990); Physica A **181**, 250 (1992).
[19] K. Binder and D. P. Landau, J. Chem. Phys. **96**, 1444 (1992).
[20] K. Binder, D. P. Landau, and A. M. Ferrenberg, Phys. Rev. Lett. **74**, 298 (1995); Binder, D. P. Landau, and A. M. Ferrenberg, Phys. Rev. E **51**, 2823 (1995).
[21] K. Binder, R. Evans, D. P. Landau, and A. M. Ferrenberg, Phys. Rev. E **53**, 5023 (1996).
[22] E. V. Albano, K. Binder, and W. Paul, J. Phys. A **30**, 3285 (1997).
[23] A. M. Ferrenberg, D. P. Landau, and K. Binder, Phys. Rev. E **58**, 3353 (1998).
[24] M. Müller, K. Binder, and E. V. Albano, Physica A **279**, 188 (2000).
[25] E. V. Albano, K. Binder, and W. Paul, J. Phys. Condens. Matter **12**, 2701 (2000).
[26] O. Dillmann, W. Janke, M. Müller, and K. Binder, J. Chem. Phys. **114**, 5823 (2001).
[27] B. J. Schulz, K. Binder, and M. Müller, Phys. Rev. E **71**, 046705 (2005).
[28] A. De Virgiliis, E. V. Albano, M. Müller, and K. Binder, Physica A **352**, 477 (2005).
[29] A. De Virgiliis, E. V. Albano, M. Müller, and K. Binder, J. Phys. Condens. Matter **17**, 4579 (2005).
[30] J. S. Rowlinson and B. Widom, *Molecular Theory of Capillarity* (Oxford University Press, Oxford, 1982).
[31] S. Dietrich, in *Phase Transitions and Critical Phenomena*, edited by C. Domb and J. L. Lebowitz, Vol. XII (Academic, New York, 1988), p. 1.
[32] G. Forgacs, R. Lipowsky, and T. M. Nieuwenhuizen, in *Phase Transitions and Critical Phenomena*, edited by C. Domb and J. L. Lebowitz, Vol. 14, Chap. 2 (Academic, New York, 1991).
[33] K. Binder and D. P. Landau, Phys. Rev. B **37**, 1745 (1988).
[34] K. Binder, D. P. Landau, and S. Wansleben, Phys. Rev. B **40**, 6971 (1989).
[35] M. Hasenbusch and K. Pinn, Physica A **203**, 189 (1994).
[36] A. O. Parry, J. M. Romero-Enrique, and A. Lazarides, Phys. Rev. Lett. **93**, 086104 (2004); L. Pang, D. P. Landau, and K. Binder, *ibid.* **106**, 236102 (2011).
[37] K. Binder and P. C. Hohenberg, Phys. Rev. B **6** (1972); **9**, 2194 (1974).
[38] H. E. Stanley, *An Introduction to Phase Transitions and Critical Phenomena* (Oxford University Press, Oxford, 1971).
[39] L. Pang, Ph.D. thesis, University of Georgia, 2010.
[40] D. P. Landau and K. Binder, *A Guide to Monte Carlo Simulation in Statistical Physics*, 3rd ed. (Cambridge University Press, Cambridge, 2009).
[41] K. Binder, Z. Phys. B **43**, 119 (1981).
[42] T. W. Burkhardt and B. Derrida, Phys. Rev. B **32**, 7273 (1985).
[43] D. P. Landau and D. Stauffer, J. Phys. **50**, 509 (1989).
[44] G. Kamienarz and H. W. Blöte, J. Phys. A **26**, 201 (1993).
[45] N. B. Wilding, J. Phys. Condens. Matter **9**, 585 (1997).
[46] J. Yin and D. P. Landau (unpublished).
[47] W. C. K. Poon, J. Phys. Condens. Matter **14**, R859 (2002).
[48] Y. Hennequin, D. G. A. L. Aarts, J. O. Indekeu, H. N. W. Lekkerkerker, and D. Bonn, Phys. Rev. Lett. **100**, 178305 (2008).